ACS APPLIED MATERIALS & INTERFACES

Research Article

www.acsami.org

A pH-Responsive Molecular Switch with Tricolor Luminescence

Hyungmin Ahn,[†] Jaewan Hong,[‡] Sung Yeon Kim,[‡] Ilyoung Choi,[‡] and Moon Jeong Park*[,†,‡]

[†]Department of Chemistry and [‡]Division of Advanced Materials Science, Pohang University of Science and Technology, Pohang 790-784, Korea

Supporting Information

ABSTRACT: We developed a new ratiometric pH sensor based on poly(*N*-phenylmaleimide) (PPMI)-containing block copolymer that emits three different fluorescent colors depending on the pH. The strong solvatochromism and tautomerism of the PPMI derivatives enabled precise pH sensing for almost the entire range of the pH scale. Theoretical calculations have predicted largely dissimilar band gaps for the keto, enol, and enolate tautomers of PPMI owing to low-dimensional conjugation effects. The tunable emission wavelength and intensity of our sensors, as well as the reversible color switching with high-luminescent contrast, were achieved using rational molecular design of PPMI analogues as an innovative platform for accurate H^+ detection. The self-assembly of block copolymers on the nanometer length scale was particularly highlighted as a novel prospective means of regulating fluorescence properties while avoiding the self-quenching phenomenon, and this system can be used as a fast responsive pH sensor in versatile device forms.

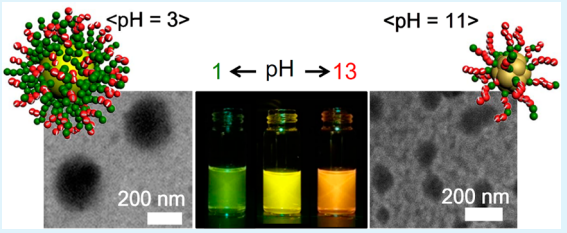

KEYWORDS: *pH sensors, fluorescence, ratiometric, tautomerism, multicolor luminescence, self-assembly*

INTRODUCTION

Recently, accurate and fast measurements of pH have become greatly important in environmental and life sciences.[1,2] This interest led to remarkable advances in electrochemical pH sensors over the past few decades.[3−5] However, optical pH sensors have now emerged as desirable gears by offering numerous advantages including improved stability, facile pH detection with the naked eye, ease of device fabrication, flexibility of design, etc.[6,7]

Most optical pH sensors developed to date can be classified as "single-wavelength" fluorescence sensors, which exploit the protonation or deprotonation of organic dyes[8−10] or quantum dots functionalized with pH-responsive polymers.[11−13] Because pH variations above or below the pK_a lead to changes in emission intensity by causing swelling or aggregation of the pH-responsive units in aqueous media, so-called "turn-off" pH sensors can be implemented. However, for practical applications, such systems have the fundamental limitations of a low signal-to-noise ratio and nonspecific interference from other substances near the sensors.[7] These limitations prompted the investigation of color-switching pH sensors based on ratiometric changes in the emission intensities with pH of two or more fluorophores.[14−17] Quantum dots should be well-suited for such purpose owing to their size-dependent emission wavelength and high quantum yield, but the quantum dots inevitably require additional functionalization of the surfaces, usually with pH-sensitive moieties.[18−21]

Compared with the thorough exploration of turn-off pH sensors, the study of color-switching pH sensors based on ratiometric emission profiles is quite limited, and thus an in-depth understanding of the underlying mechanism of ratiometric pH sensors at the molecular level is still in its infancy. One facile route to develop ratiometric pH sensors is the noncovalent immobilization of fluorophores that emit at different wavelengths in a polymer matrix, therefore avoiding laborious synthetic steps.[22−24] Another suitable approach is the confinement of one type of organic dye in the nanodomains of a polymer to induce longer wavelength excimer emission in response to pH changes.[25,26] Despite the simplicity of the aforementioned systems, leaching of the fluorophores from the polymer matrix in various sensing environments was problematic and impeded long-term reliable use of the sensors.[27] In addition, precise control over the ratio of fluorophores and their distribution in the polymer matrix to obtain ratiometric color changes remain a challenging task.

In this respect, covalent attachment of multiple chromophores to a polymer matrix by post-treatment[28,29] or direct polymerization of different fluorophore-bearing monomer units[30,31] has drawn intensive attention in recent years. A challenge of this approach is the incorporation of pH sensitivity into such polymers. Work on pH sensors based on conjugated polymers modified with ionizable moieties[32,33] has taken advantage of the tremendous growth seen for decades in the field of conjugated polymers.[34,35] Although several functionalized conjugated polymers showed promising pH-tunable light emission properties,[36−38] ratiometric pH sensors derived from conjugated polymers have the shortcoming of a narrow pH-sensing window.[39,40] Good processability to integrate the conjugated polymer into various devices with stable signals is also crucial for a state-of-the-art ratiometric pH sensor.

Received: October 13, 2014
Accepted: December 23, 2014
Published: December 23, 2014

DOI: 10.1021/am5070188
ACS Appl. Mater. Interfaces 2015, 7, 704−712

However, success has seldom been reported because of the uncontrolled aggregation of chromophores that causes a large decline in emission efficiency. The development of a new type of ratiometric pH sensor, based on unprecedented polymers, that is easy to synthesize, does not require incorporation of dyes, and emits in more than two wavelength regions with reversible emission colors over a wide range of pH values would have great impact.

Herein, we report a new ratiometric pH sensor made of mass-produced engineering plastic derivatives that emits three different colors (green, yellow, orange), subject to pH changes. *N*-phenylmaleimide (PMI) was employed as a monomer unit, and the synthesized poly(*N*-phenylmaleimide) (PPMI) belongs to a class of commercially available polymaleimides. The strong solvatochromism and tautomerism of PPMI were responsible for the notable tricolor switching behavior with pH, which was the basis of the wide and precise pH-sensing window. To date, the spectroscopic consequences of tautomerism in small molecules[41,42] or in vinyl polymers bearing tautomerizable moieties[43,44] have been investigated, but those of polymers themselves have not been reported. Time-dependent density functional theory (TDDFT) calculations revealed that each tautomer possessed largely dissimilar band gaps, with a total band gap shift of 3.4 eV.

We also demonstrate precise control of the fluorescence properties by designing PPMI analogues substituted with an electron-withdrawing or electro-donating group, which offers a generic and effective strategy for developing sensors with tunable light-emitting wavelengths and intensities. In particular, the facile synthesis of a PPMI-containing block copolymer enabled us to achieve good water solubility, unique self-assembled morphology that avoided uncontrolled aggregation, and easy processability into various device forms (solutions, thin films, and even membranes). This system lends itself to versatile sensor designs and thus paves the way for unprecedented access to future sensor technologies.

EXPERIMENTAL SECTION

Synthesis of Poly(*N*-phenylmaleimide) (PPMI, 1a) and Its Analogues with Chlorine (1b) or Ethyl (1c) Substituents. *N*-phenylmaleimide (TCI), *N*-(2,4,6-trichlorophenyl)maleimide (TCI), and *N*-(4-ethylphenyl)maleimide (Alfa-Aesar) were purified by recrystallization from toluene/cyclohexane (50/50 vol %), followed by sublimation under reduced pressure. **1a**, **1b**, and **1c** were synthesized by anionic polymerization of each monomer at room temperature for 24 h; 2 g of purified monomer was dissolved in 200 mL of distilled toluene, and the reaction was initiated by injecting 0.2 mL of potassium *tert*-butoxide (1.0 M in tetrahydrofuran (THF)). The reaction was terminated with methanol, and the polymer in the reaction mixture was purified by repeated precipitations in methanol and dialysis against pure water using a cellulose dialysis membrane with a 3.5 kg/mol molecular weight cutoff (VWR) for 10 d. The polymer was then recovered by vacuum drying at 60 °C for 7 d. The molecular weights and molecular weight distributions of **1a**, **1b**, and **1c** were characterized by combining ^{1}H nuclear magnetic resonance (^{1}H NMR, Bruker AVB-300) spectroscopy and gel permeation chromatography (GPC, Waters Breeze 2 HPLC). The polydispersity indices (PIs) of the polymers were less than 1.35.

Synthesis of Poly(ethylene oxide-*b*-*N*-phenylmaleimide) (PEO-*b*-PPMI, 2a). Poly(ethylene glycol) methyl ether (MPEG, M_n = 2.0 kg/mol) was purchased from Aldrich and used without further purification. **2a** was synthesized by anionic polymerization using activated MPEG as a macroinitiator; 1.5 g of MPEG was dissolved in 200 mL of purified THF, and sodium naphthalide (0.1 M in THF) was slowly injected to the mixture under argon. Activated MPEG macroinitiators are indicated by a light green color. *N*-phenylmaleimide (0.75 g) was then transferred to the reaction mixture and allowed to react for 48 h at room temperature. The reaction was terminated with methanol, and the polymer in the reaction mixture was purified by repeated precipitations in ether and dialysis against pure water using a cellulose dialysis membrane with a 3.5 kg/mol molecular weight cutoff (VWR) for 10 d. The polymer was then recovered by vacuum drying at 60 °C for 7 d. The PI of PEO-*b*-PPMI was 1.13.

Characterization of Fluorescence Properties. The UV−visible spectra of the solutions of **1a**, **1b**, and **1c** homopolymers and **2a** block copolymer were measured using an Agilent 8453 UV−visible spectrophotometer. Fluorescence spectra of the solutions were recorded on a Shimadzu-RF5301PC spectrofluorophotometer. The emission spectra were recorded after exciting the solutions at the wavelength of 445 nm. The pH-sensing experiments were carried out by monitoring the fluorescence intensities of aqueous **2a** solutions after the injection of different concentrations of H^+ or OH^- at room temperature. Fluorescence photographs of thin films and membranes were taken under irradiation at 445 nm using LED lamp at room temperature.

Absorption Spectra, Oscillator Strengths, Molecular Orbitals, Band Gaps, and ^{1}H NMR Shift Calculations. The analysis of electronic structures of the **1a** tautomers was undertaken using TDDFT with the B3PW91/6-31G** hybrid functional in Gaussian 09 for which the geometry had been optimized in THF.

Morphology Study. The micellar morphologies of **2a** in aqueous media were investigated by combining dynamic light scattering, zetapotential measurements, and transmission electron microscopy (TEM) experiments. The time-intensity autocorrelation functions, $g^2(\tau)$, of the solutions were accumulated by logarithmic digital correlator at a scattering angle of 173°. Each correlation function decayed to the baseline (within 0.1% or better). Distributions of decay rates were obtained by fitting with a combination of exponential functions. Zeta potentials were obtained from electrophoretic mobility (μ_e) measurements (Malvern Zetasizer Nano system) using the Hückel approximation with irradiation from a 633 nm He−Ne laser using a combination of electrophoresis and laser Doppler velocimetry techniques. The μ_e is measured from the rate of transport of an ion under an applied electric field and for accurate determination, where all μ_e values presented in this work are average values of five different measurements with relative spans less than 0.3%. All solutions were filtered using 0.45 μm pore size filters to avoid the effect of impurity. For TEM analysis, samples were prepared by drop-coating of the solutions on Formvar-coated TEM grids. The samples were dried at room temperature for 2 d under a N_2 blanket, followed by vacuum drying at 40 °C for 3 d. Imaging of dried and unstained samples was performed with a Hitachi H-800 microscope operating at 80 kV equipped with a Gatan 2048 × 2048 pixel CCD camera. (Gatan Inc., Pleasanton, CA).

Preparation of Sensors in Forms of Thin Films and Membranes. Inhibitor-free anhydrous THF (≥99.9%) was used without further purification. Predetermined quantities of polymers were weighted into glass vials, and 5 wt % solutions were prepared using THF. Thin films with ca. 500 nm thickness were prepared by drop-casting on glass substrates, followed by vacuum drying at 60 °C for 2 d. For the fabrication of freestanding membranes with ca. 300 μm thickness, polyethylene glycol diacrylate (PEGDA, M_n = 700, Sigma-Aldrich) was employed. The mixture of **2a** and PEGDA (75/25 wt %) was dissolved in chlorobenzene at a concentration of 1 wt % and ball milled for 5 min. Two types of photoinitiators, 2-hydroxy-2-methyl-1-phenyl-1-propanone (HMPP, Sigma-Aldrich) and Lucirin TPO (BASF), were then added to the solution, wherein the concentration of HMPP and TPO was 1 wt % of PEGDA. The mixture was immediately dropped on quartz and UV-cured for 20 s using an LED UV lamp (Phoseon, 2000 mW/cm^2).

RESULTS AND DISCUSSION

Luminescent PPMI and Its Substituted Analogues. Figure 1a shows the synthetic procedure for PPMI (**1a**) and its

DOI: 10.1021/am5070188
ACS Appl. Mater. Interfaces 2015, 7, 704−712

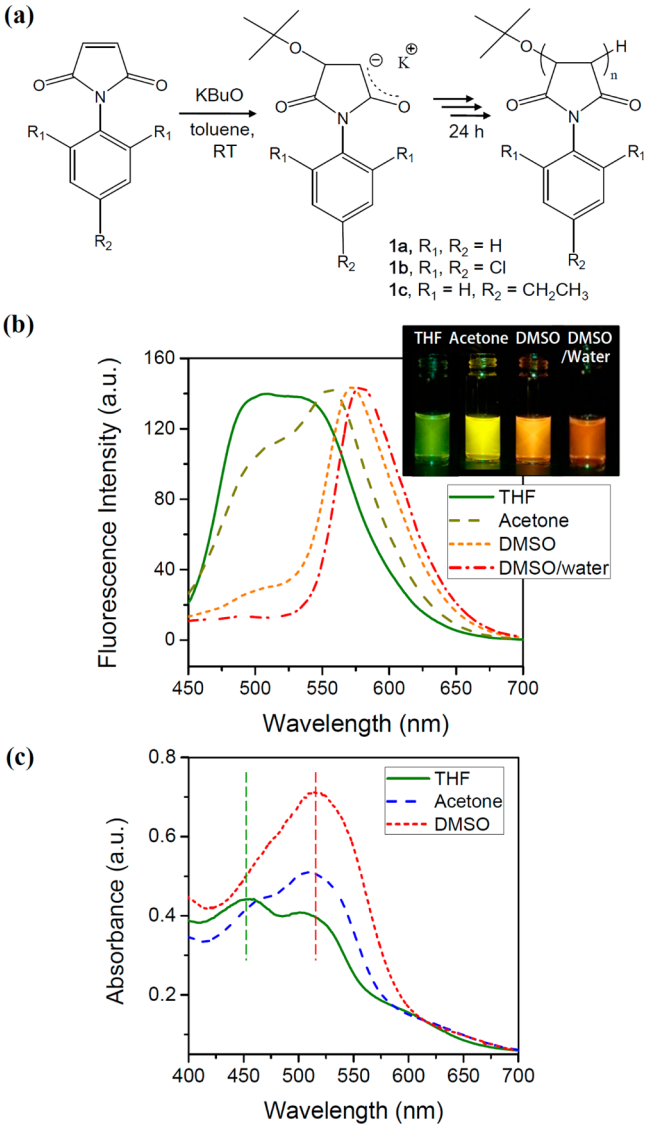

Figure 1. (a) Synthetic procedure for PPMI (**1a**) and its analogues with chlorine (**1b**) or ethyl (**1c**) substituents. (b) Fluorescence emission intensities (excited at 445 nm) and (c) UV–vis absorption spectra of 0.2 wt % **1a** in different solvents. The inset photographs in (b) were obtained under irradiation at 445 nm.

analogues with chlorine (**1b**, poly(*N*-(2,4,6-trichlorophenylmaleimide)) or ethyl (**1c**, poly(*N*-(4-ethylphenylmaleimide)) substituents. The as-synthesized **1a** (7.5 kg/mol), **1b** (5.2 kg/mol), and **1c** (7.8 kg/mol) polymers were pink powders with crystalline characteristics. Detailed information of the synthesized polymers is provided in Figure S1 of Supporting Information. **1a**, **1b**, and **1c** showed good solubility in many organic solvents such as benzene, THF, dichloromethane, acetone, dimethylformamide, and dimethyl sulfoxide (DMSO).

Upon dissolving **1a** in the aforementioned solvents, the solutions showed strong fluorescence emission under UV irradiation, and the emission color was largely dependent on the solvent polarity. Figure 1b shows representative fluorescence spectra of 0.2 wt % **1a** in four different solvents: THF (solid line), acetone (dash line), DMSO (short dash line), and DMSO/water (50/50 vol %, dash-dot line). The solvent polarity parameters, $E_T(30)$, of THF, acetone, DMSO, and DMSO/water are 37.4, 42.2, 45.1, and 55.6 kcal/mol, respectively.[45] As can be seen in Figure 1b, two overlapped peaks of similar intensities at 490 and 545 nm, corresponding to green and yellow-green fluorescence, respectively, were observed in THF (the solvent with the lowest polarity). In acetone, the fluorescence intensity of the green emission was reduced, and the yellow-green emission was red-shifted to 560 nm. In DMSO, the green emission was significantly decreased, and orange emission with a maximum wavelength of 573 nm was dominant. The fluorescence quantum yield of **1a** in THF, acetone, and DMSO was calculated as 11%, 9%, and 5%, respectively. The solvent polarity was further increased using a cosolvent of water and DMSO, and fluorescence emission centered at 580 nm was observed. Photographs of the solutions, taken under irradiation at 445 nm, are shown in the inset of Figure 1b, further revealing that **1a** in THF, acetone, DMSO, and DMSO/water displays green, yellow, orange, and deep orange luminescence, respectively. We note here that the PMI monomer did not exhibit detectable fluorescence in any solvent.

Interestingly, luminescence of **1a** is not expected for the keto form of PPMI, as drawn in Figure 1a, owing to the nonconjugated character. In particular, the positive solvatochromism with a significant red shift of 90 nm observed for the fluorescence emission wavelength suggested that the more polar environments stimulated the energy differences in electronic states of **1a** toward lower values. In support of this conjecture, we show the UV absorption spectra of **1a** in THF, acetone, and DMSO in Figure 1c. Two absorption peaks with similar intensities were observed at wavelength maxima (λ_{max}) of 452 and 503 nm for **1a** in THF. The absorption intensity at short wavelength was gradually reduced with an increase in solvent polarity, and a dominant absorption band centered at 514 nm was observed for **1a** in DMSO. In Figure S2 of Supporting Information, the plots of λ_{max} versus $E_T(30)$ for **1a** in seven different solvents are given, indicating the increase in λ_{max} with solvent polarity for short- and long-wavelength absorption. We infer that two absorption peaks of **1a** solutions are resulted from two different ground-state species, where their populations are depending on the solvent polarity.

We infer that tautomerism in **1a** played a central role in the observed multicolor fluorescence as the equilibriums among keto, enol, and enolate tautomers are influenced by the polarity of the environment. To gain quantitative insights into the multicolor-emitting behavior of **1a**, analysis of electronic structures of the **1a** tautomers was undertaken using TDDFT with the B3PW91/6-31G** hybrid functional in Gaussian 09 for which the geometry had been optimized in THF. Figure 2a presents representative chemical structures of the keto, enol, and enolate forms of **1a**. The predicted λ_{max} and oscillator strengths of the tautomers with a degree of polymerization (N) of **2** are summarized in Table 1. It can be deduced that the short-wavelength absorption was produced by enolization, whereas the longer wavelength absorption is originated from the deprotonation of the enol. In THF, the enol and enolate tautomers coexist, while the population of enolate increases with increasing solvent polarity due to excited-state proton-transfer reaction, resulting in the gradual red shifts in the λ_{max} (Figure 1c and Supporting Information, Figure S2). This was confirmed by calculating the λ_{max} of enol–enolate (50–50) mixture; the λ_{max} values lie in order enol < enol–enolate (50–50) < enolate. A maximum Stokes shift of 184 nm in the absorption spectra of **1a** was predicted for complete ionization, which is far greater than that observed experimentally. Note

DOI: 10.1021/am5070188
ACS Appl. Mater. Interfaces 2015, 7, 704–712

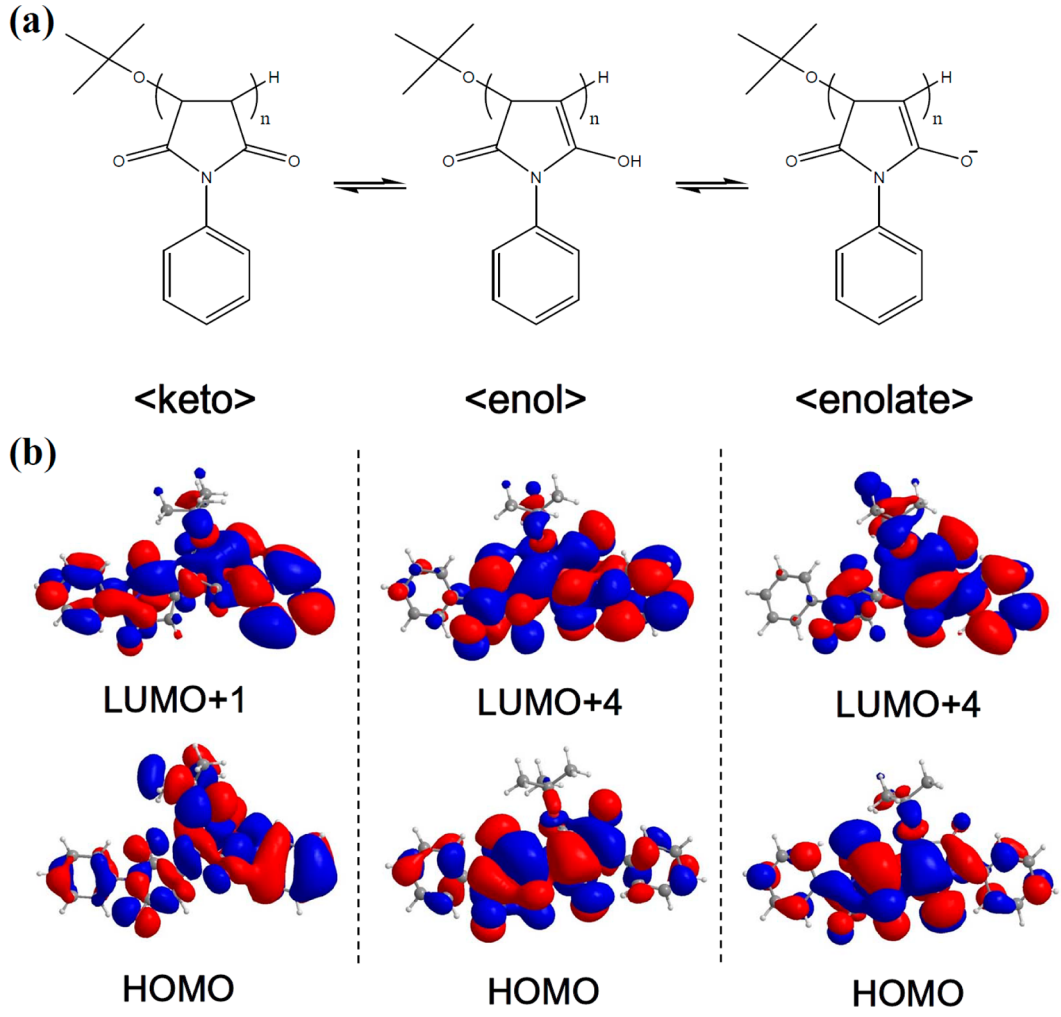

Figure 2. (a) Chemical structures and (b) HOMO and LUMO morphologies of **1a** in forms of keto, enol, and enolate.

Table 1. Calculated Absorption Spectra (λ_{max}), Oscillator Strengths (f), and Dominant Excitation Configurations and Energies Predicted for the 1a in THF with TDDFT B3PW91/6-31G**

absorption spectra			composition of λ_{max}				
tautomer	λ_{max}	f	dominant excitation	probability (%)	HOMO (eV)	LUMO (eV)	ΔE (eV)
keto	247	0.0583	HOMO → LUMO+1	18.8	−6.63	−0.69 (LUMO+1)	5.95
enol	335	0.4656	HOMO → LUMO+4	47.7	−4.53	−0.34 (LUMO+4)	4.19
enolate	431	0.2061	HOMO → LUMO+4	48.5	−1.72	1.75 (LUMO+4)	3.47
enol−enolate (50−50)	352	0.3776	HOMO → LUMO+4	47.0	−0.78	3.25 (LUMO+4)	4.03

here that although the keto form is part of the equilibrium, it is nonfluorescent, and thus the equilibrium between the keto and enol was not determined by fluorescence spectra.

Figure 2b shows the highest occupied molecular orbital (HOMO) and the lowest unoccupied molecular orbital (LUMO) morphologies of the **1a** tautomers. For the enol and enolate tautomers, the dominant electronic transition in the absorption was HOMO → LUMO+4 as determined at the B3PW91/6-31G** level, while that for the keto tautomer was HOMO → LUMO+1, as listed in Table 1. Overall, the nature of the HOMO and LUMO depended on the presence of the conjugated dienes because of their strong electron-withdrawing effect.[46] For the keto tautomer, an antibonding interaction between PMI repeat units was observed that stabilized the HOMO. On the contrary, the HOMOs in the enol and enolate resided mainly on the maleimide units accompanied by an antibonding orbital between the phenyl ring and the maleimide ring. The localized π-electrons within the maleimide unit led to the increase of the HOMO energies of the enol and enolate owing to the low-dimensional conjugation effects. In particular, the charged oxygen atoms of the enolate enhanced electron-donating effects[46] and yielded a destabilized HOMO with increased energy. These effects resulted in the decreasing HOMO−LUMO gaps observed, from 5.95 (keto) to 4.19 (enol) to 3.47 eV (enolate), as listed in Table 1. We note that since the molecular weight of **1a** employed in the present study is much larger (N = 43) than that of the calculated model (N = 2), many experimental parameters such as polydispersity in chain length and compositional fluctuations can further decrease the band gap.[47] In the Supporting Information (Table S1 and Figure S3), we have provided extended λ_{max} values and HOMO−LUMO band gaps for **1a** tautomers.

DOI: 10.1021/am5070188
ACS Appl. Mater. Interfaces 2015, 7, 704−712

Taking into consideration the easy modification of **1a** ring structure, we attempted to change the distribution of electron density in the **1a** without significantly expanding the geometry. These modifications were made to manipulate the chemical equilibrium of the keto, enol, and enolate tautomers of **1a** and thereby regulate the fluorescence properties in a straightforward manner. Figure 3a presents fluorescence intensities of **1a**, **1b**, and **1c** in THF. The fluorescence wavelengths and intensities were greatly influenced by the substituents, that is, electron-withdrawing (**1b**) or electron-donating (**1c**) moieties, yielding bright green and yellow emissions for **1b** and **1c**, respectively (see inset photographs, Figure 3a).

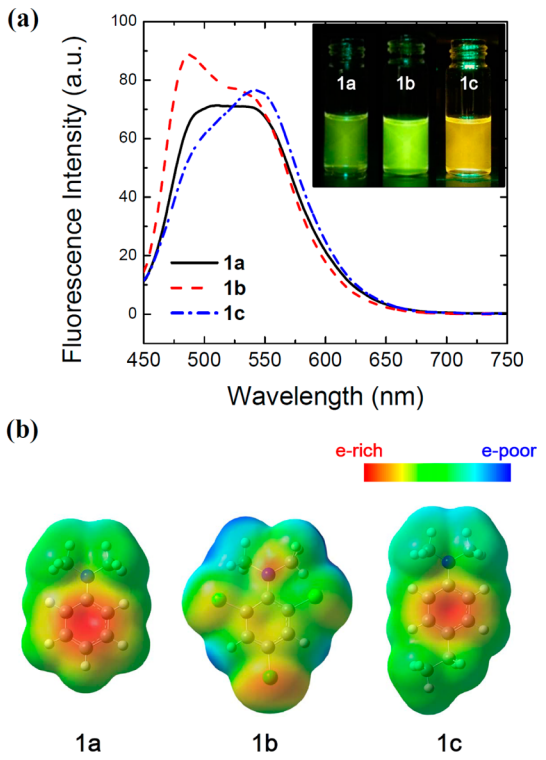

Figure 3. (a) Fluorescence intensities of **1a**, **1b**, and **1c** in THF at a concentration of 0.2 wt %. The inset photographs in (a) were obtained under irradiation at 445 nm. (b) Electrostatic surface potentials calculated for *N*,*N*-dimethylaniline of **1a**, **1b**, and **1c** by ab initio calculation using DFT (using 6-31G* basis sets).

The spectral changes observed for **1b** and **1c** compared with **1a** in THF were a consequence of the different proton-donating abilities of enol tautomer depending on the substituents. Namely, the introduction of the Cl substituents in **1b** stabilized the enol tautomer (chemical equilibrium shift from keto tautomer) by reducing the electron density within the maleimide units. However, the ground-state enolate tautomer was observed with introduction of the ethyl substituent in **1c**. This can be rationalized by resonance structure of phenyl ring, that is, the reduced electron density at the nitrogen atom upon the attachment of electron-donating ethyl group to the ring, which eventually increased the electron density at the oxygen atom. Electrostatic surface potentials were calculated for *N*,*N*-dimethylaniline of **1a**, **1b**, and **1c** by ab initio calculations using DFT with the B3LYP/6-31G* hybrid functional in Gaussian 09, as shown in Figure 3b. The alterations in electron densities within phenyl rings and nitrogen atoms were apparent by attaching electron-withdrawing Cl (**1b**) or electron-donating ethyl (**1c**) moieties, which led to the stabilization of the enol or enolate, respectively.

Multicolor Emission of PPMI with the Addition of Acid or Base. On the basis of the assumption that a basic solution would facilitate the ionization of the enol group, we examined the possibility of using our PPMI derivatives to develop acid/base responsive fluorescent materials. We examined the tuning of the fluorescence properties of **1a** upon the addition of acid or base to solution. Figure 4a,b shows the fluorescence intensities and UV–vis spectra for **1a** in THF, respectively, with the addition of H^+ or OH^- to the solution. Overall, the solution showed stronger emission in basic conditions, whereas a significant reduction in the fluorescence intensity was detected with the addition of acid. Interestingly, the green emission was significantly decreased in the presence of OH^-, but there was no change in the emission maximum of 490 nm. On the contrary, the fluorescence intensity of the yellow emission increased with the increasing concentration of OH^-, concomitantly with a red shift in the emission maximum, which was stabilized at orange fluorescence with an emission wavelength of 570 nm when 1 mM of OH^- was added. It is inferred that the increase in basicity of the solution caused an increase in the proportion of the enolate due to deprotonation of the enol. From the UV–vis spectra shown in Figure 4b, we confirmed the acid/base sensitivity of the ground-state

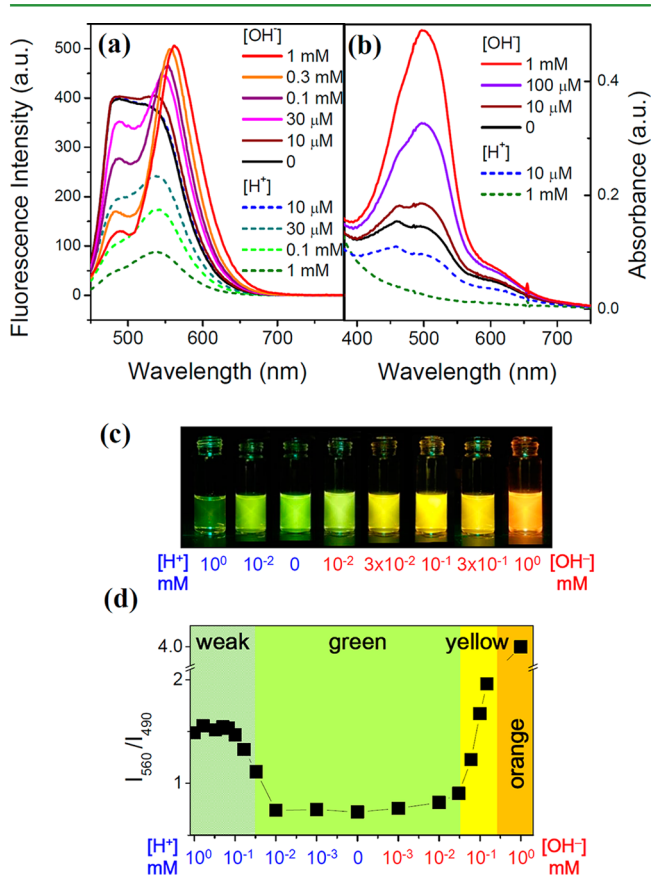

Figure 4. (a) Fluorescence intensities (excited at 445 nm) and (b) UV–vis absorption spectra for 0.2 wt % **1a** in THF with the addition of H^+ or OH^- to the solution. (c) The photographs taken under irradiation at 445 nm and (d) the fluorescence intensity ratios of the two emission maxima at 560 and 490 nm (I_{560}/I_{490}) as a function of acid/base concentration are shown to illuminate three color regimes.

DOI: 10.1021/am5070188
ACS Appl. Mater. Interfaces 2015, 7, 704–712

equilibriums of **1a** in THF; the intensities of the two absorption peaks decreased in acidic conditions, whereas the absorption at long-wavelength was notably enhanced with an increase in basicity.

The acid/base sensitive fluorescence of **1a** in THF can be clearly observed in the photographs taken under UV irradiation, as shown in Figure 4c. For further quantitation of the system, the fluorescence intensity ratios of the two emission maxima at 560 and 510 nm (I_{560}/I_{510}) were plotted as a function of $[H^+]/[OH^-]$ concentration in Figure 4d. Notably, three color regimes were observed in the figures, with transitions at $[H^+]$ of 0.03 mM and $[OH^-]$ of 0.03 mM. Weak fluorescence was observed in acidic conditions ($[H^+]$ > 0.03 mM), green emission was observed at intermediate acidity and basicity with virtually no change in intensity ratio, yellow emission was observed in the $[OH^-]$ window 0.03−0.3 mM due to the concurrent decrease in green and increase in orange emission, and orange emission was observed as a high "turn on" response in strongly basic conditions ($[OH^-]$ > 0.3 mM). The first transition at $[H^+]$ of 0.03 mM should be associated with self-quenching by the aggregation of fluorophores in strongly acidic conditions. After this transition the coexistence of the enol and enolate at a constant ratio was anticipated from the similar values of I_{560}/I_{490} in the intermediate acidity and basicisity. The ionization of the enol was ultimately stimulated by increasing the pH, as seen by the second transition at $[OH^-]$ of 0.03 mM.

Note that the acid/base sensitivity of the fluorescence of **1a** was determined by the interplay between the basicity and the polarity of the solvent. For **1a** in DMSO, for example, the dominant orange emission centered at 580 nm was almost insensitive to the addition of acid or base to the solution. Plots of λ_{max} versus $[H^+]/[OH^-]$ concentration for **1a** in THF and DMSO displaying the dissimilar transition points are provided in Figure S4 of Supporting Information.

Ratiometric pH Sensor Developed from a Water-Soluble Block Copolymer. Finally, we explored ways to utilize the acid/base responsive fluorescence properties of **1a** in practical applications, that is, as a pH sensor. Since the essential property for the use of a material in a pH sensor is water solubility, we designed a new polymer, poly(ethylene oxide-*b*-*N*-phenylmaleimide) (PEO-*b*-PPMI, 2.0-*b*-2.1 kg/mol) block copolymer, composed of fluorescent **1a** and water-soluble PEO chains with an optimized composition. Hereafter, the PEO-*b*-PPMI block copolymer is referred to as **2a**. The molecular structure of **2a** is shown in Figure 5a (detailed molecular characteristics of **2a** are provided in Figure S5 of Supporting Information).

Figure 5b represents the pH-sensitive fluorescence of **2a** in aqueous media. While the tricolor emitting properties were conserved, as shown in the inset photographs, several notable differences between **2a** and **1a** were seen from the emission spectra: (1) In highly acidic conditions, contrary to the dominant quenching behavior of **1a**, strong green emission was observed for the aqueous solution of **2a**, indicating that the covalently bound hydrophilic PEO chains alleviated uncontrolled aggregation of PPMI moieties at low pH. (2) The maxima of the green emission was red-shifted to 510 nm for **2a**, compared to 490 nm for **1a**, indicating a decrease in the emission energy of the **2a** enol tautomer. (3) Unlike the single color luminescence observed for **1a** in polar environments (Figure 1b), **2a** revealed dual-emission properties in neutral aqueous solution. With the increase in pH, the enhancement of the long-wavelength fluorescence emission at 570 nm was fairly

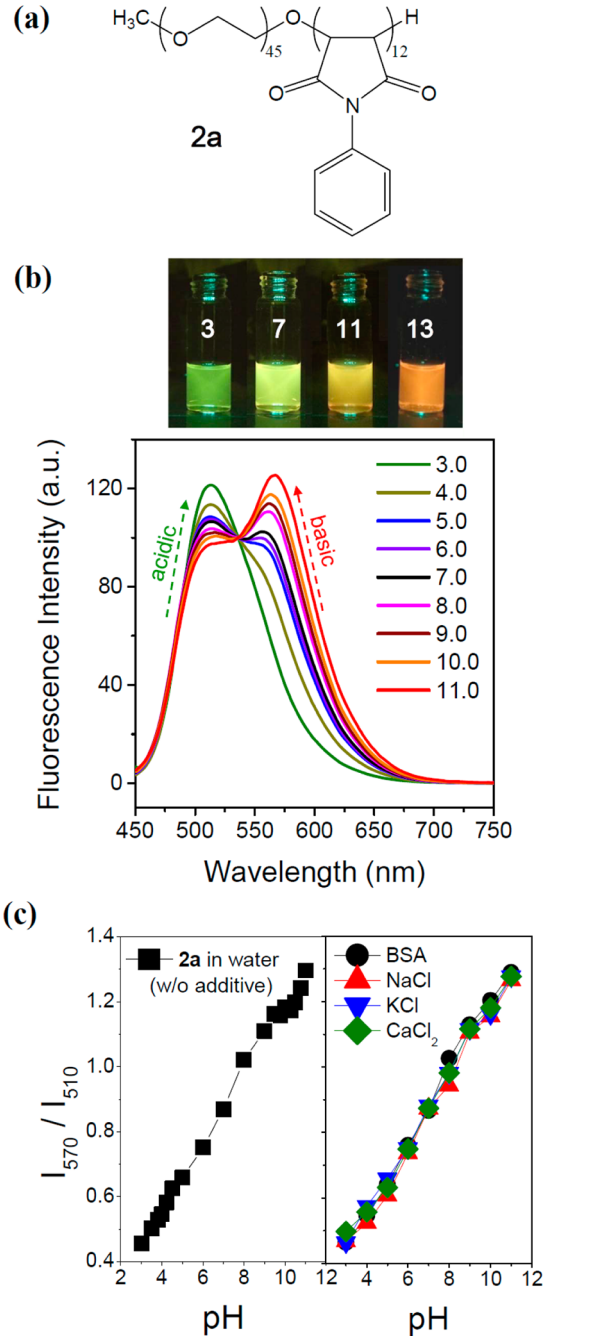

Figure 5. (a) Molecular structure of **2a**. (b) Fluorescence intensities and photographs (taken under irradiation at 445 nm) of 0.2 wt % **2a** in aqueous media at different pH conditions. (c) The fluorescence intensity ratios of the two emission maxima at 570 and 510 nm (I_{570}/I_{510}) vs pH, revealing ratiometric fluorescence behavior over almost the entire pH range. The I_{570}/I_{510} vs pH of the solutions upon the addition of bovine serum albumin (30 μg/mL) or different salts (NaCl, KCl, $CaCl_2$, 100 μM) are also compared in (c).

modest, and the dual emission was preserved in strongly basic conditions. This result indicated that complete conversion to the enolate was not obtained for **2a** even in highly polar and basic environments.

To quantitatively determine the pH-sensing performance of multicolor-emitting **2a**, the fluorescence intensity ratio of the two emission maxima at 570 and 510 nm (I_{570}/I_{510}) was plotted as a function of pH in Figure 5c. To our surprise, unlike **1a**, **2a**

DOI: 10.1021/am5070188
ACS Appl. Mater. Interfaces 2015, 7, 704−712

in aqueous media demonstrates ratiometric fluorescent behavior over almost the entire pH range, indicated by the linear relationship between I_{570}/I_{510} and the pH. Such a wide pH-sensing window is considered to be of importance for practical applications but has rarely been reported in the literature. Given that selective and stable recognition of $[H^+]$ over competing species is of significance importance, we further examined the fluorescence intensities of **2a** in aqueous media upon the addition of bovine serum albumin (BSA) or a range of salts (NaCl, KCl, and $CaCl_2$). As compared in Figure 5c, the I_{570}/I_{510} of the solutions after the addition of BSA or salts bears resemblance to that of the original solution. This suggests the possible uses of our sensor in biological environments with nonsignificant interference from other substances.

To find the reasons behind the observed advance, the morphology of **2a** in aqueous media at different pH conditions was elucidated. Spherical micellar morphology was observed for the solutions, where the size of the micelles was significantly influenced by the solution pH. Representative TEM images of the micelles of **2a**, obtained at pH values of 3, 7, and 11, are shown in Figure 6a. Uniformly sized spherical micelles were evident at pH 3 and 7, whereas the micelles become disrupted/fused at pH 11. Interestingly, a 2-fold larger micelle was observed under acidic conditions, compared with those at pH 7, while the micelles become smaller with an increase in basicity. This result indicated that the hydrophobic attraction/electrostatic repulsion balance was shifted by the pH changes, where dominant electrostatic repulsion between charged enolate tautomers at high pH caused instability of the micelles. Schematic drawings illustrating the micellar morphology of **2a** in aqueous media are depicted in inset graphics of Figure 6a.

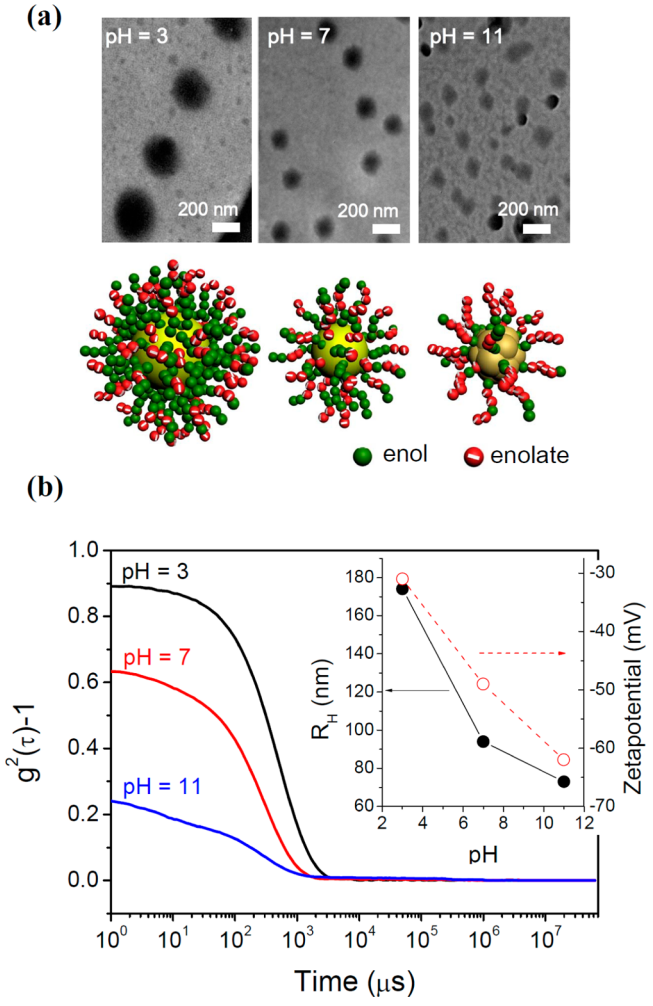

Figure 6. (a) TEM micrographs of the micelles of 0.2 wt % **2a** in aqueous media at different pH conditions. Schematic illustrations depicting pH-sensitive micellar morphologies are given in the inset graphics of (a). (b) Time-intensity correlation functions of 0.2 wt % aqueous **2a** solutions obtained at pH = 3, 7, and 11. pH-sensitive radii and zeta potentials of the micelles are plotted in the inset of (b).

We also performed dynamic light scattering (DLS) experiments for 0.2 wt % aqueous solutions of **2a** by varying pH. The DLS correlation curves are shown in Figure 6b, where the gradual disruption of micelles with the increase in pH was clearly revealed. The hydrodynamic radius of the micelle was determined as 174 (pH 3), 94 (pH 7), and 73 nm (pH 11), in good agreement with the TEM results. To further identify where the PPMI chains were located in the micelles, electrophoretic measurements were carried out. Judging from negative potentials of the micelles at all pH values, the micellar corona appeared to be composed of partially ionized PPMI chains, as schematically depicted in Figure 6a. The high selectivity of water for enolate is responsible for the location despite the hydrophilic characteristics of PEO. As plotted in the inset of Figure 6b, pH-sensitive zeta potentials of the micelles, that is, −31 (pH 3), −49 (pH 7), and −62 mV (pH 11), imply that the degree of ionization increases moderately at higher pH values owing to the steric hindrance of the charged PPMI confined within the micelles. This effect is ascribed to the preserved dual-emission properties even in the presence of excessive amounts of OH^-.

Stability, reversibility, and response time are key factors in evaluating a pH sensor. As shown in Figure 7a, reversible color switching and high luminescent contrast were demonstrated for the aqueous solution of **2a** over multiple cycles (fluorescence intensities are given in Figure S6 of Supporting Information). The use of **2a** as a pH sensor is not limited to solutions. We developed **2a** as a pH sensor in versatile devices to highlight the novelty of the present study compared with systems reported in the literature. Figure 7b represents the pH-sensing properties of a thin film of **2a** with ca. 500 nm thickness upon exposure to a few drops of water with different pH values. The fast color-switching behavior among green, yellow, and orange fluorescence was demonstrated for the thin film, where the time to complete the change in signal was less than 30 s. This was attributed to the unique tautomerism of our sensor as a pH-sensing mechanism. We provided a video in the Supporting Information to demonstrate the rapid changes in the pH sensing signals of **2a** in the form of a film.

In addition, when **2a** was produced as a 300 μm thick freestanding membrane with the aid of a UV-curable polymer, the sensor revealed analogous fluorescent color changes when soaked in aqueous solutions of different pH values, as shown in Figure 7c. It is thus clear that self-quenching behavior was negligible in **2a** regardless of the final form, making **2a** applicable to convenient, inexpensive, and versatile sensor designs. Note that by taking advantage of the high molecular weight characteristics of polymers to create effective entangled networks, the membrane sensor demonstrated negligible leaching of **2a** molecules even when immersed in water for a few months.

The main aim of our present study was to open a new chapter in ratiometric pH sensors by proposing an innovative

DOI: 10.1021/am5070188
ACS Appl. Mater. Interfaces 2015, 7, 704−712

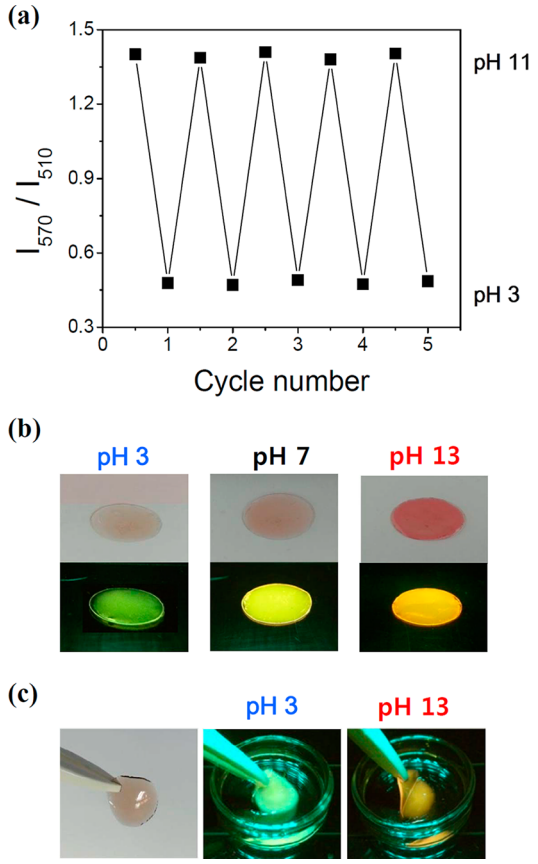

Figure 7. (a) Reversible changes in the fluorescence intensity ratios of the two emission maxima at 570 and 510 nm (I_{570}/I_{510}) with step changes in pH. Fluorescence micrographs of (b) thin film and (c) freestanding membrane of **2a** at pH = 3 (green) and pH = 13 (orange), taken with LED illumination.

design for a light-emitting polymer with a pH-sensitive chemical equilibrium. The strengths of our sensor, compared to a vast number of works on fluorescent pH sensors, can be summarized as follows: (1) the unique tricolor luminescent behavior with the tunable emission wavelength and intensity without any fluorescent labeling, (2) the selective and reversible detection of [H^+] with a rapid response time of <30 s in aqueous media without significant interference from other substances, and (3) the fabrication of sensors in versatile device forms with excluded self-quenching behavior. Experiments are currently underway on the application of these polymers to the development of red-emitting pH sensors by tethering different functional groups with tunable electron affinity.

CONCLUSIONS

A set of PPMI-based polymers was synthesized, and their fluorescence properties were investigated. Three different fluorescence colors of green, yellow, and orange were observed for the PPMI polymer solutions by varying solvent polarity and pH. Tautomerism of PPMI was responsible for the multicolor emitting behavior, where the chemical equilibriums among the tautomers were shifted by the interplay between pH and polarity of the solvent. Spectral changes in the luminescence were easily attained by modifying the distribution of electron density in the PPMI units via simple substitution, enabling us to find a synergetic means of developing a pH sensor with a tunable emission wavelength and intensity. In particular, upon synthesizing a water-soluble PPMI-containing block copolymer, fascinating pH-sensitive micellar morphology was obtained in aqueous media. The self-quenching phenomenon at low pH was eliminated in the block copolymer through avoidance of uncontrolled aggregation. Notably, the sensor made of PPMI-containing block copolymer demonstrated reversible ratiometric tricolor switching behavior with high luminescent contrast over almost the entire range of the pH scale. The success of this system stemmed from nanoconfinement effects, which effectively tailored electrostatic interactions, steric hindrance, and chemical equilibriums with a fast response time. The easy processing of this material into versatile device forms highlighted the promising prospects of our sensors for future pH sensors.

ASSOCIATED CONTENT

Supporting Information

GPC chromatograms and ^{1}H NMR spectra for **1a** and **2a**, λ_{max} versus $E_T(30)$ of **1a** in different solvents, extended TDDFT calculations of **1a** in forms of different tautomers, absorbance maxima and fluorescence intensities of **1a** in different solvents, fluorescence intensities of aqueous **2a** solutions with the addition of H^+ and OH^- for multiple cycles, and a movie clip demonstrating fast response time of our sensor. This material is available free of charge via the Internet at http://pubs.acs.org.

AUTHOR INFORMATION

Corresponding Author

*E-mail: moonpark@postech.edu.

Notes

The authors declare no competing financial interest.

ACKNOWLEDGMENTS

This work was financially supported by National Nuclear R&D Program (2011-0031931), the Global Frontier R&D program on Center for Multiscale Energy System funded by the National Research Foundation under the Ministry of Science, ICT & Future, Korea.

REFERENCES

(1) Korostynska, O.; Arshak, K.; Gill, E.; Arshak, A. Review on State-of-the-art in Polymer Based pH Sensors. *Sensors* **2007**, *7*, 3027−3042.
(2) Krulwich, T. A.; Sachs, G.; Padan, E. Molecular Aspects of Bacterial pH Sensing and Homeostasis. *Nat. Rev. Microbiol.* **2011**, *9*, 330−343.
(3) Ang, P. K.; Chen, W.; Wee, A. T. S.; Loh, K. P. Solution-Gated Epitaxial Graphene as pH Sensor. *J. Am. Chem. Soc.* **2008**, *130*, 14392−14393.
(4) Xu, B.; Zhang, W.-D. Modification of Vertically Aligned Carbon Nanotubes with RuO_2 for a Solid-State pH Sensor. *Electrochim. Acta* **2010**, *55*, 2859−2864.
(5) Santos, L.; Neto, J. P.; Crespo, A.; Nunes, D.; Costa, N.; Fonseca, I. M.; Barquinha, P.; Pereira, L.; Silva, J.; Martins, R.; Fortunato, E. WO_3 Nanoparticle-Based Conformable pH Sensor. *ACS Appl. Mater. Interfaces* **2014**, *6*, 12226−12234.
(6) Wencel, D.; Abel, T.; McDonagh, C. Optical Chemical pH Sensors. *Anal. Chem.* **2014**, *86*, 15−29.
(7) Fenzi, C.; Wilhelm, S.; Hirsch, T.; Wolfbeis, O. S. Optical Sensing of the Ionic Strength Using Photonic Crystals in a Hydrogel Matrix. *ACS Appl. Mater. Interfaces* **2013**, *5*, 173−178.
(8) Baruah, M.; Qin, W.; Basarić, N.; Borggraeve, W. M. D.; Boens, N. BODIPY-Based Hydroxyaryl Derivatives as Fluorescent pH Probes. *J. Org. Chem.* **2005**, *70*, 4152−4157.

DOI: 10.1021/am5070188
ACS Appl. Mater. Interfaces 2015, 7, 704−712

(9) Ke, G.; Zhu, Z.; Wang, W.; Zou, Y.; Guan, Z.; Jia, S.; Zhang, H.; Wu, X.; Yang, C. J. A Cell-Surface-Anchored Ratiometric Fluorescent Probe for Extracellular pH Sensing. *ACS Appl. Mater. Interfaces* **2014**, *6*, 15329−15334.
(10) You, S.; Cai, Q.; Mullen, K.; Yang, W.; Yin, M. pH-Sensitive Unimolecular Fluorescent Polymeric Micelles: from Volume Phase Transition to Optical Response. *Chem. Commun.* **2014**, *50*, 823−825.
(11) Wu, Y.; Chakrabortty, S.; Gropeanu, R. A.; Wilhelmi, J.; Xu, Y.; Er, K. S.; Kuan, S. L.; Koynov, K.; Chan, Y.; Weil, T. pH-Responsive Quantum Dots via an Albumin Polymer Surface Coating. *J. Am. Chem. Soc.* **2010**, *132*, 5012−5014.
(12) Medintz, I. L.; Stewart, M. H.; Trammell, S. A.; Susumu, K.; Delehanty, J. B.; Mei, B. C.; Melinger, J. S.; Blanco-Canosa, J. B.; Dawson, P. E.; Mattoussi, H. Quantum-Dot/Dopamine Bioconjugates Function as Redox Coupled Assemblies for *in vitro* and Intracellular pH Sensing. *Nat. Mater.* **2010**, *9*, 676−684.
(13) Frasco, M. F.; Chaniotakis, N. Semiconductor Quantum Dots in Chemical Sensors and Biosensors. *Sensors* **2009**, *9*, 7266−7286.
(14) Fan, J.; Hu, M.; Zhan, P.; Peng, X. Energy Transfer Cassettes Based on Organic Fluorophores: Construction and Applications in Ratiometric Sensing. *Chem. Soc. Rev.* **2013**, *42*, 29−43.
(15) Chen, S.; Hong, Y.; Liu, Y.; Liu, J.; Leung, C. W.; Li, M.; Kwok, R. T.; Zhao, E.; Lam, J. W.; Yu, Y.; Tang, B. Z. Full-Range Intracellular pH Sensing by an Aggregation-Induced Emission-Active Two-Channel Ratiometric Fluorogen. *J. Am. Chem. Soc.* **2013**, *135*, 4926−4929.
(16) Shi, W.; Li, X.; Ma, H. A Tunable Ratiometric pH Sensor Based on Carbon Nanodots for the Quantitative Measurement of the Intracellular pH of Whole Cells. *Angew. Chem., Int. Ed.* **2012**, *124*, 6538−6541.
(17) Wan, S.; Zheng, Y.; Shen, J.; Yang, W.; Yin, M. ″On-off-on″ Switchable Sensor: A Fluorescent Spiropyran Responds to Extreme pH Conditions and Its Bioimaging Applications. *ACS Appl. Mater. Interfaces* **2014**, *6*, 19515−19519.
(18) Dennis, A. M.; Rhee, W. J.; Sotto, D.; Dublin, S. N.; Bao, G. Quantum Dot-Fluorescent Protein FRET Probes for Sensing Intracellular pH. *ACS Nano* **2012**, *6*, 2917−2924.
(19) Snee, P. T.; Somers, R. C.; Nair, G.; Zimmer, J. P.; Bawendi, M. G.; Nocera, D. G. A Ratiometric CdSe/ZnS Nanocrystal pH Sensor. *J. Am. Chem. Soc.* **2006**, *128*, 13320−13321.
(20) Hu, X.; Gao, X. Silica-Polymer Dual Layer-Encapsulated Quantum Dots with Remarkable Stability. *ACS Nano* **2010**, *4*, 6080−6086.
(21) Zhang, R.; Zhao, D.; Ding, H.-G.; Huang, Y.-X.; Zhong, H.-Z.; Xie, H.-Y. Sensitive Single-Color Fluorescence "off−on" Switch System for dsDNA Detection Based on Quantum Dots-Ruthenium Assembling Dyads. *Biosens. Bioelectron.* **2014**, *56*, 51−57.
(22) Wencel, D.; MacCraith, B. D.; McDonagh, C. High Performance Optical Ratiometric Sol-Gel-Based pH Sensor. *Sens. Actuators, B* **2009**, *139*, 208−213.
(23) Peng, H.-S.; Stolwijk, J. A.; Sun, L.-N.; Wegener, J.; Wolfbeis, O. S. A Nanogel for Ratiometric Fluorescent Sensing of Intracellular pH Values. *Angew. Chem., Int. Ed.* **2010**, *122*, 4342−4345.
(24) Wang, X.-D.; Stolwijk, J. A.; Lang, T.; Sperber, M.; Meier, R. J.; Wegener, J.; Wolfbeis, O. S. Ultra-Small, Highly Stable, and Sensitive Dual Nanosensors for Imaging Intracellular Oxygen and pH in Cytosol. *J. Am. Chem. Soc.* **2012**, *134*, 17011−17014.
(25) Sun, G.; Cui, H.; Lin, L. Y.; Lee, N. S.; Yang, C.; Neumann, W. L.; Freskos, J. N.; Shieh, J. J.; Dorshow, R. B.; Wooley, K. L. Multicompartment Polymer Nanostructures with Ratiometric Dual-Emission pH-Sensitivity. *J. Am. Chem. Soc.* **2011**, *133*, 8534−8543.
(26) Zhang, X.; Rehm, S.; Safont-Sempere, M. M.; Würthner, F. Vesicular Perylene Dye Nanocapsules as Supramolecular Fluorescent pH Sensor Systems. *Nat. Chem.* **2009**, *1*, 623−629.
(27) Chan, Y.-H.; Wu, C.; Ye, F.; Jin, Y.; Smith, P. B.; Chiu, D. T. Development of Ultrabright Semiconducting Polymer Dots for Ratiometric pH Sensing. *Anal. Chem.* **2011**, *83*, 1448−1455.
(28) Kumar, E. K. P.; Almdal, K.; Andresen, T. L. Synthesis and Characterization of Ratiometric Nanosensors for pH Quantification: A Mixed Micelle Approach. *Chem. Commun.* **2012**, *48*, 4776−4778.
(29) Lee, N. S.; Sun, G.; Lin, L. Y.; Neumann, W. L.; Freskos, J. N.; Karwa, A.; Shieh, J. J.; Dorshow, R. B.; Wooley, K. L. Tunable Dual-Emitting Shell-Crosslinked Nano-Objects as Single-Component Ratiometric pH-Sensing Materials. *J. Mater. Chem.* **2011**, *21*, 14193−14202.
(30) Koopmans, C.; Ritter, H. Color Change of N-Isopropylacrylamide Copolymer Bearing Reichardts Dye as Optical Sensor for Lower Critical Solution Temperature and for Host-Guest Interaction with-Cyclodextrin. *J. Am. Chem. Soc.* **2007**, *129*, 3502−3503.
(31) Wan, X.; Liu, S. Fluorescent Water-Soluble Responsive Polymers Site-Specifically Labeled with FRET Dyes Possessing pH- and Thermo-Modulated Multicolor Fluorescence Emissions as Dual Ratiometric Probes. *J. Mater. Chem.* **2011**, *21*, 10321−10329.
(32) Wang, M.; Zou, S.; Guerin, G.; Shen, L.; Deng, K.; Jones, M.; Walker, G. C.; Scholes, G. D.; Winnik, M. A. A Water-Soluble pH-Responsive Molecular Brush of Poly(*N*,*N*-dimethylaminoethyl methacrylate) Grafted Polythiophene. *Macromolecules* **2008**, *41*, 6993−7002.
(33) Thomas, S. W., III; Joly, G. D.; Swager, T. M. Chemical Sensors Based on Amplifying Fluorescent Conjugated Polymers. *Chem. Rev.* **2007**, *107*, 1339−1386.
(34) McQuade, D. T.; Pullen, A. E.; Swager, T. M. Conjugated Polymer-Based Chemical Sensors. *Chem. Rev.* **2000**, *100*, 2537−2574.
(35) Jiang, H.; Taranekar, P.; Reynolds, J. R.; Schanze, K. S. Conjugated Polyelectrolytes: Synthesis, Photophysics, and Applications. *Angew. Chem., Int. Ed.* **2009**, *48*, 4300−4316.
(36) Xu, Q.; An, L.; Yu, M.; Wang, S. Design and Synthesis of a New Conjugated Polyelectrolyte as a Reversible pH Sensor. *Macromol. Rapid Commun.* **2008**, *29*, 390−395.
(37) Rugen-Penkalla, N.; Klapper, M.; Müllen, K. Highly Charged Conjugated Polymers with Polyphenylene Backbones and Poly(acrylic acid) Side Chains. *Macromolecules* **2012**, *45*, 2301−2311.
(38) Jo, S.; Kim, D.; Son, S.-H.; Kim, Y.; Lee, T. S. Conjugated Poly(fluorene-quinoxaline) for Fluorescence Imaging and Chemical Detection of Nerve Agents with Its Paper-Based Strip. *ACS Appl. Mater. Interfaces* **2014**, *6*, 1330−1336.
(39) Kim, I.-B.; Phillips, R.; Bunz, U. H. F. Carboxylate Group Side-Chain Density Modulates the pH-Dependent Optical Properties of PPEs. *Macromolecules* **2007**, *40*, 5290−5293.
(40) Wang, F.; Bazan, G. C. Aggregation-Mediated Optical Properties of pH-Responsive Anionic Conjugated Polyelectrolytes. *J. Am. Chem. Soc.* **2006**, *128*, 15786−15792.
(41) Naumov, P.; Kochunnoonny, M. Spectral-Structural Effects of the Keto-Enol-Enolate and Phenol-Phenolate Equilibria of Oxyluciferin. *J. Am. Chem. Soc.* **2010**, *132*, 11566−11579.
(42) Xu, Z.; Baek, K.-H.; Kim, H. N.; Cui, J.; Qian, X.; Spring, D. R.; Shin, I.; Yoon, J. Zn^{2+}-Triggered Amide Tautomerization Produces a Highly Zn^{2+}-Selective, Cell-Permeable, and Ratiometric Fluorescent Sensor. *J. Am. Chem. Soc.* **2010**, *132*, 601−610.
(43) Wen, Q.; Liu, L.; Yang, Q.; Lv, F.; Wang, S. Dopamine-Modified Cationic Conjugated Polymer as a New Platform for pH Sensing and Autophagy Imaging. *Adv. Funct. Mater.* **2013**, *23*, 764−769.
(44) Yang, C.-C.; Tian, Y.; Chen, C.-Y.; Jen, A. K. -Y.; Chen, W.-C. A Novel Benzoxazole-Containing Poly(*N*-isopropylacrylamide) Copolymer as a Multifunctional Sensing Material. *Macromol. Rapid Commun.* **2007**, *28*, 894−899.
(45) Reichardt, C. Solvatochromic Dyes as Solvent Polarity Indicators. *Chem. Rev.* **1997**, *94*, 2319−2358.
(46) Roncali, Z. Synthetic Principles for Bandgap Control in Linear π-Conjugated Systems. *Chem. Rev.* **1997**, *97*, 173−205.
(47) Ahn, H.; Kim, S.; Kim, O.; Choi, I.; Lee, C.-H.; Shim, J. H.; Park, M. J. Blue-emitting Self-assembled Polymer Electrolytes for Fast, Sensitive, Label-free Detection of Cu(II)-ions in Aqueous Media. *ACS Nano* **2013**, *7*, 6162−6169.

DOI: 10.1021/am5070188
ACS Appl. Mater. Interfaces 2015, 7, 704−712